Range-Coplanarity equation for radar geometric imaging

CHENG Chunquan[1], ZHANG Jixian[1], DENG Kazhong[2], ZHANG Li[1]

1. *Chinese Academy of Surveying and Mapping*, *Beijing* 100039, *China*;
2. *China University of mining and Technology*, *Xuzhou* 221116, *China*

Abstract: Geometric imaging equation is the most fundamental and important formula for photogrammetry, and rigorousness and conciseness are main factors constrain its applicability. In this paper, following the analyzing of attitude influence on side-looking radar imaging, a rigorous and concise geometric imaging equation based on Range-Coplanarity (R-Cp) condition is proposed using positions and attitudes (e.g., exterior orientation elements) of the radar sensor as orientation parameters. The equation considers the effect of attitude angles on radar image positioning, reflects the imaging geometric principle of radar images in both distance and azimuth directions, removes the complicated imaging parameters, and realizes the coherence of orientation parameters of rigorous model for optical image and side-looking radar image. Furthermore, it also shows higher positioning experiment precision compared to Konecny G model and Leberl F model. Theory and tests indicate that the equation has potential applications in the field of photogrammetry on radar remote sensing images.

Key words: range-coplanarity equation, geometric imaging equation, exterior orientation elements, side-looking radar, rigorous sensor model

CLC number: P237 **Document code:** A

Citation format: Cheng C Q, Zhang J X, Deng K Z and Zhang L . 2012. Range-Coplanarity equation for radar geometric imaging. Journal of Remote Sensing, 16(1): 38–49

1 INTRODUCTION

The rigorous geometric imaging model of side-looking radar image mainly includes the range doppler equation and the radar collinearity equation (Chen, 2004). Leberl F model proposed by Leberl F (Leberl, 1978, 1990), according to range condition and zero doppler condition, complies with the radar imaging mechanism. It takes into account of the changes in line elements of exterior orientation of the sensor, while without considering the effects of angular elements. The R-D model, with similar mechanism of Leberl F model, takes into account of the non-zero value situation of doppler frequency which is often expressed by constants, linearity, or low order polynomial model on different image points, and therefore has explicit geometric and physical meaning (Johnsen, et al., 1995). Based on the R-D model, many scholars have studied the positioning of SAR images, including models without control points (Zhu, et al., 2003; Yang, et al., 2006), a few control points (Yuan & Wu, 2010) and for high mountainous areas (Gelautz, et al., 1998; Johnsen, et al., 1995). The radar collinearity equation-based model, using exterior orientational elements as its orientation parameters, is the extension of the application of collinearity equation in optical remote sensing image. The collinearity equation, proposed by Konecny and Schuhr (1988), includes the influence of topography of the ground point (Konecny & Schuhr, 1988). Rigorous collinearity equation for radar image are also used by modifying the approximate collinearity equation through the conversion of range projection to center projection (You, 2007; Li, et al., 2007), and to build the geometric imaging model based on exterior orientation elements.

2 INFLUENCE OF ATTITUDE ON RADAR IMAGING

In R-D model, attitude parameters are not involved. The mechanism of roll angle on radar imaging and image positioning is always in dispute in the academic field (Pang, 2006). In this study, the independent influence of each attitude angle is briefly analyzed first, and then an clear conclusion about the influence of roll angle on radar image positioning is reached in the derivation process of Coplanarity equation.

Fig. 1(a) shows the ideal condition where all the three attitude angles are zero. With real aperture radar taken as the observing object, the influence of attitude angular changes on the imaging and image positioning is analyzed comparing to the ideal condition.

Received: 2011-05-22; **Accepted:** 2011-07-31

Foundation: National Natural Science Foundation of China (No.41071237); National High Technology Research and Development program of China (863 program) (No.2011AA120401, 2011AA120402); Leading Talent Fund of State Bureau of Surveying and Mapping (No. A11114)

First author biography: CHENG Chunquan (1972—), male, Ph.D., associate professor, his research interests are digital photogrammetry of optical and SAR images. E-mail:cspring@casm.ac.cn

2.1 Influence of roll angle (ω) on the radar imaging

The presence of roll angle changes the surveying scope of radar antenna. But for the same ground point, the photographic time of the ground point is not changed, and the range between the radar antenna and the ground point at photography time also remains unchanged. Therefore, with two other attitude angles being constant, the changes only in roll angle does not affect the radar imaging for a given object, as shown in Fig. 1(b).

2.2 Influence of pitch angle (φ) on the radar imaging

The presence of pitch angle causes forward and backward displacement of the ground object with reference to radar sensor position at the photography time, thus the shoot time for the same ground point changes, and the range between ground point and the radar antenna increases. Therefore, the changes in pitch angle lead to the variations in image row and column coordinates of ground points, affecting the imaging and image positioning, as shown in Fig. 1(c).

2.3 Influence of yaw angle (κ) on the radar imaging

The presence of yaw angle leads to the deflexion of beam center, thus the photographic time for the same ground point changes and the range between ground point and the sensor antenna increases. Therefore, image coordinates of the ground point will change accordingly, and the change of row coordinate varies significantly according to column coordinates or the range, its indicate that the yaw angle have direct influence on imaging for radar image ,as shown in Fig. 1(d).

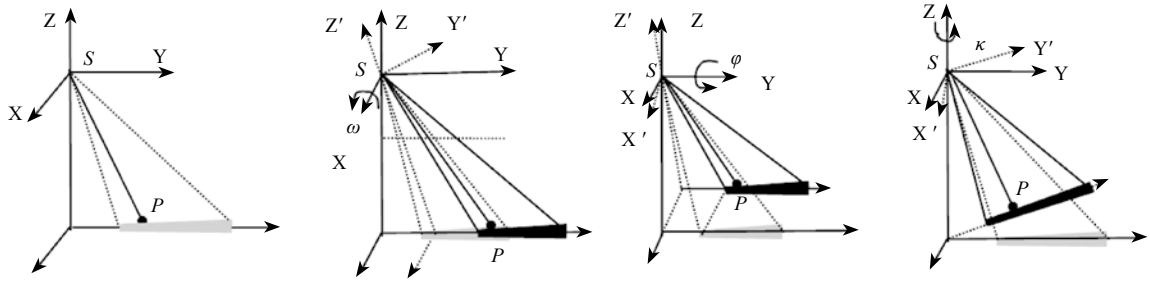

(a) Attitude angles are zero values (b) Influence of roll angle (c) Influence of pitch angle (d) Influence of yaw angle

Fig. 1 Schematic diagram of the influence of attitude angles on the positioning of side-looking radar image

3 RANGE-COPLANARITY EQUATION FOR THE POSITIONING OF SIDE-LOOKING RADAR IMAGE

Side-looking radar has two modes, namely planar scanning and conical scanning (Shu, 2000). Here the planar scanning is firstly discussed.

3.1 Fundamental principles of R-Cp equation

The range-coplanarity condition refers to that all the ground points corresponding to one line in the image are within the scanning central plane of radar beam emitted by antenna at the photographic time, and imaging of each pixel in the row meets the range conditions (Fig. 2). The geometric imaging equation of radar remote sensing image based on the state vector and the attitude parameters (e.g., exterior orientation elements) is constructed through range conditions between sensor and objects, and coplanarity condition of radar beam center:

(1) All ground points corresponding to one line in image and the radar antenna at shoot time are within one center plane of radar beam, which is determined by state vector and attitude of the sensor.

(2) The spatial range between sensor and ground points is equal to the range measured by radar wave.

Range-coplanarity condition is established by the following equations:

$$\begin{cases} R = |\overrightarrow{OP} - \overrightarrow{OS}| = \tau c / 2 \\ \vec{i} \cdot (\overrightarrow{OP} - \overrightarrow{OS}) = 0 \end{cases} \quad (1)$$

where $\vec{i}$ is the normal vector of the plane of radar beam center (the same as x′ axis which is converted from x axis in the sensor coordinate system by rotating attitude angles), $\overrightarrow{OP}$, $\overrightarrow{OS}$ are the position vectors of ground points and the radar antenna, respectively. R is the slant distance; c is the speed of light; τ is the round-trip time of radar beam from antenna to the ground point. The first formula is range equation, which is identical to the range equation both in R-D model and in Leberl F model. The second formula is plane equation of radar beam center.

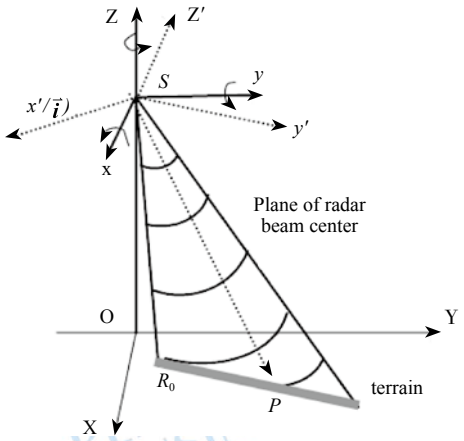

Fig. 2 Range-coplanarity imaging geometry of side-looking radar

3.2 Selection of rotation angle system and the coplanarity equation of planar scanning mode

The influence of attitudes on side-looking radar image positioning has already been analyzed in the previous section through independent study of three attitude angles. The conclusion can been

drawn that φ and κ influence the imaging and image positioning, while ω only influences the surveying scope rather than image positioning. Because the latter rotation of euler angle is based on the former rotation, influence of ω on the radar image positioning also depends on the rotation sequence. Euler angles have 6 rotation sequences. In optical image positioning, ω-φ-κ system is mostly used internationally. However, this rotation sequence is not applicable in building coplanarity equation of radar images, which can be demonstrated in the following formula derivation.

3.2.1 Scanning plane with ω-φ-κ system

Through the rotation of attitude angles of ω-φ-κ system, the rotation matrix $\boldsymbol{R}_b^A$ of the conversion from body coordinate system of the sensor to object-space reference coordinate system is as follows.

$$\boldsymbol{R}_b^A = \boldsymbol{R}_X(\omega)\boldsymbol{R}_Y(\varphi)\boldsymbol{R}_Z(\kappa) \tag{2}$$

For the normal vector of scanning plane of radar beam corresponds to x' axis of sensor coordinate system after attitude rotation, its unit vector in the object-space coordinate system is derived as follows.

$$\vec{\boldsymbol{i}} = \boldsymbol{R}_b^A \begin{bmatrix} 1 \\ 0 \\ 0 \end{bmatrix} = \begin{bmatrix} \cos\varphi\cos\kappa \\ \cos\omega\sin\kappa + \sin\omega\sin\varphi\cos\kappa \\ \sin\omega\sin\kappa - \cos\omega\sin\varphi\cos\kappa \end{bmatrix} \tag{3}$$

Substitute the Eq. (3) into Eq. (1). (X_S, Y_S, Z_S) and (X, Y, Z) are used to represent the spatial coordinates of the sensor and the ground point, respectively. Then, a new formula is derived as follows.

$$\begin{aligned}&(X-X_S)\cos\varphi\cos\kappa+(Y-Y_S)(\cos\omega\sin\kappa+\sin\omega\sin\varphi\cos\kappa)+\\&(Z-Z_S)(\sin\omega\sin\kappa-\cos\omega\sin\varphi\cos\kappa)=0\end{aligned} \tag{4}$$

3.2.2 Scanning plane with φ-κ-ω system

φ-κ-ω system successively take Y-Z-X axes as its rotation sequence, with the attitude rotation matrix as follows.

$$\boldsymbol{R}_b^A = \boldsymbol{R}_Y(\varphi)\boldsymbol{R}_Z(\kappa)\boldsymbol{R}_X(\omega) \tag{5}$$

The unit vector of the normal line of scanning plane in object-space coordinate system is as follows.

$$\vec{\boldsymbol{i}} = \boldsymbol{R}_b^A \begin{bmatrix} 1 \\ 0 \\ 0 \end{bmatrix} = \begin{bmatrix} \cos\varphi\cos\kappa \\ \sin\kappa \\ -\sin\varphi\cos\kappa \end{bmatrix} \tag{6}$$

Similarly, this formula is substituted into the coplanarity equation in Eq. (1). Then the expansion formula is obtained as follows.

$$\begin{aligned}&(X-X_S)(\cos\varphi\cos\kappa)+(Y-Y_S)\sin\kappa-\\&(Z-Z_S)(\sin\varphi\cos\kappa)=0\end{aligned} \tag{7}$$

It can also demonstrate that when κ-φ-ω rotation angle system is adopted, ω is not involved in coplanarity equation as Eq. (7).

3.2.3 Range-coplanarity equation of side-looking radar of planar scanning mode

The range equation in R-Cp equations is identical to that in the R-D equation, and together with coplanarity Eq. (7) constitutes slant distance-based R-Cp equation:

$$\begin{cases}(X-X_S)(\cos\varphi\cos\kappa)+(Y-Y_S)\sin\kappa-\\\qquad\qquad(Z-Z_S)(\sin\varphi\cos\kappa)=0\\(X-X_S)^2+(Y-Y_S)^2+(Z-Z_S)^2=(y_sM_y+R_0)^2\end{cases} \tag{8}$$

where M_y is the resolution of slant range direction; R_0 is the initial slant distance; y_s is the column coordinate of pixel in the image.

It can be seen from the derivation of coplanarity equation that when ω-φ-κ rotation angle system is adopted, ω impacts image positioning; when φ-κ-ω rotation angle system is adopted, ω has no impact on image positioning. R-Cp equations which adopt φ-κ-ω rotation angle system are constructed using three line elements and two angle elements as orientation parameters. When attitude angles have different values, coplanarity equation represents the aggregate of different planes passing sensor antenna position at the shoot time. When the plane is perpendicular to the direction of sensor velocity, then the corresponding R-Cp equation model becomes the model proposed by Leberl F. Thus, Leberl F model can be treated as a special case of the R-Cp model.

With identical state vector of the sensor (position and velocity) and same topography, different attitudes of radar sensor will lead to different doppler frequency, and attitude parameters and doppler parameters are mutually convertible. Similar to all types of radar collinearity equation model, R-Cp model uses attitude angles as parameter, without direct association with such parameters as doppler frequency and radar wavelength. This indicates that the geometric processing of radar image is possible by avoiding the imaging parameters. For a non-side-looking radar, different pixels in one line image have different doppler frequencies, but they have the same group of attitude angles. There is tight link as well as disparity between R-Cp model and R-D model.

3.3 Radar imaging equation of conical scanning

When side-looking radar works according to the conical scanning mode, radar beam has a constant tilt τ, and it makes conical scanning by revolving around the antenna axis, as shown in Fig. 3 (Shu, 2000).

Any ground point P must be on the scanning conical surface, with R as the range between the point and the sensor. Equation for conical surface could be build according to the angle value between two vectors, i.e., vector $\vec{\boldsymbol{r}}$, which is constituted by all of the ground points and the locations of antenna, and vector $\vec{\boldsymbol{i}}$ of rotation axis, is 90° – τ. Therefore, the mathematical expression for the conical surface is as follows.

$$\cos(\vec{\boldsymbol{i}},\vec{\boldsymbol{r}}) = \cos(\pi/2-\tau) = \sin(\tau) = \frac{\vec{\boldsymbol{i}}\cdot\vec{\boldsymbol{r}}}{|\vec{\boldsymbol{i}}||\vec{\boldsymbol{r}}|} \tag{9}$$

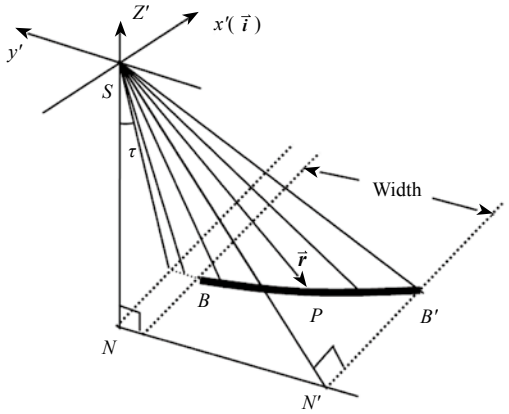

Fig. 3 Imaging geometry for radar image of conical scanning

When φ-κ-ω rotation angle system is adopted, the unit vector $\vec{\boldsymbol{i}}$ of rotation axis of the antenna in Eq. (9) is substituted by Eq. (6), thus the expansion equation of imaging equation for radar image of conical scanning is correspondingly obtained as follows.

$$\begin{cases} \cos\varphi\cos\kappa(X-X_S)+\sin\kappa(Y-Y_S)- \\ \sin\varphi\cos\kappa(Z-Z_S)-(y_sM_y+R_0)\sin\tau=0 \\ (X-X_S)^2+(Y-Y_S)^2+(Z-Z_S)^2-(y_sM_y+R_0)^2=0 \end{cases} \quad (10)$$

Since conical scanning is relatively rare, only the basic equation is presented here without in-depth discussion. In the following section, we only focus on the planar scanning.

4 RIGOROUS POSITIONING MODEL FOR RADAR REMOTE SENSING IMAGE

Based on Eq. (8), taking the elements of exterior orientation and the coordinates increment of ground points as unknown parameters and linearizing the R-Cp equations, we can establish the general form of error equation as follows.

$$\begin{cases} v_1=f_{1X_S}\delta_{X_S}+f_{1Y_S}\delta_{Y_S}+f_{1Z_S}\delta_{Z_S}+f_{1\varphi}\delta_\varphi+ \\ \quad f_{1\kappa}\delta_\kappa+f_{1X}\delta_X+f_{1Y}\delta_Y+f_{1Z}\delta_Z-l_1 \\ v_2=f_{2X_S}\delta_{X_S}+f_{2Y_S}\delta_{Y_S}+f_{2Z_S}\delta_{Z_S}+f_{2\varphi}\delta_\varphi+ \\ \quad f_{2\kappa}\delta_\kappa+f_{2X}\delta_X+f_{2Y}\delta_Y+f_{2Z}\delta_Z-l_2 \end{cases} \quad (11)$$

where v_1 and v_2 are the error equations, which respectively correspond to the range equation and coplanarity equation in Eq. (8); $f_{..}$ is the coefficient of linearization; δ is the unknown parameter of increment and its subscripts (X_S, Y_S, Z_S, φ, κ) represent the elements of exterior orientation, subscripts (X, Y, Z) represent the coordinates of ground points; l_1 and l_2 are the constants of error equations.

The refined models of exterior orientation elements are usually in the form of low-order polynomial, i.e., the formula as follows.

$$P_i=P_{i0}+a_{i0}+a_{i1}t+a_{i2}t^2+\cdots+a_{in}t^n \ (i=1, 2, 3, 4, 5) \quad (12)$$

where P_i and P_{i0} (i=1, 2, 3, 4, 5) are the refined values and initial values of position and attitude (X, Y, Z, φ, κ), respectively; (a_{i0}, a_{i1}, a_{i2}, ⋯, a_{in}) are the coefficients of general polynomial.

Combined with all error equations related to R-Cp equation, ground point coordinates, orbit and attitude, the refined model constitutes the equation set below:

$$\begin{cases} \boldsymbol{V}_{12}=\boldsymbol{B}_g\boldsymbol{g}+\boldsymbol{B}_t\boldsymbol{t}-\boldsymbol{L}_{12} & \boldsymbol{P}_{12} \\ \boldsymbol{V}_g=\boldsymbol{E}_g\boldsymbol{g}-\boldsymbol{L}_g & \boldsymbol{P}_g \\ \boldsymbol{V}_t=\boldsymbol{E}_t\boldsymbol{t}-\boldsymbol{L}_t & \boldsymbol{P}_t \end{cases} \quad (13)$$

where $\boldsymbol{V}_{12}$,$\boldsymbol{V}_g$ and $\boldsymbol{V}_t$ are the corrected vectors for the observation and virtual observation value of R-Cp conditions, ground point coordinates and POS refinement model, respectively; $\boldsymbol{g}$ is unknown parameter of the increment vector [ΔX,ΔY,ΔZ] of ground point coordinates; $\boldsymbol{t}$ is unknown parameter vector of the refinement model coefficients of POS data; $\boldsymbol{L}_{12}$, $\boldsymbol{L}_g$ and $\boldsymbol{L}_t$ are the corresponding constant vectors of error equation, respectively; $\boldsymbol{B}_g$, $\boldsymbol{B}_t$, $\boldsymbol{E}_g$ and $\boldsymbol{E}_t$ are the design matrixes of error equation coefficients; $\boldsymbol{P}_{12}$, $\boldsymbol{P}_g$ and $\boldsymbol{P}_t$ are weight matrixes.

5 EXPERIMENT

Imaging equation has been applied in nearly field of aerial and space photogrammetry. In this study, the imaging equations are verified to be accurate and are feasible only by positioning model. The error equations of combined-adjustment used in both orientation and positioning are Eq. (13), i.e. R-Cp equation is constructed based on φ-κ-ω rotation angle system. The orientation parameters are calculated by least square solutions; the theoretical values of ground check point coordinates are calculated by orientation parameters; and the accuracy of ground check point coordinates is calculated by the error statistics between theoretical value and observation values. The airborne SAR images used as experimental data were acquired in June, 2006 in the area of Chengdu. The sampling resolutions of both azimuth direction and range direction of image pixel are 1.0 m, and the actual ground resolution of the images is about 2.5 m. The adopted POS system was AV510 produced by Applanix Corporation of Canada. Due to the large time synchronization error between POS system and sensor at the early days of system integration, GPS data are used as initial observation values after their rough errors are offset by constants, while the initial attitude values are set as zero.

5.1 Orientation experiment of single-view image

There are altogether 14 ground points with known coordinates in the image area, which are acquired through aerial triangulation by high-resolution optical aerial images. The original image and the distribution of ground points are shown in Fig. 4.

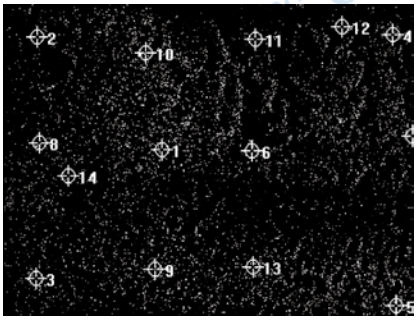

Fig. 4 Airborne SAR image and ground points

1 GCP (central control,Point No.1), 2 GCPs (control at upper left corner and lower right corner), 4 GCPs (quadrangle control), 9GCPs (control at three rows and three columns) and 13 GCPs (LOOCV assess precision method, (Brovelli M,et al., 2006), in which all of the ground points are successively selected as check points) are respectively adopted in image positioning. When 13 GCPs are used, quadratic polynomial is adopted as refined model of POS data, while the linear refined model is adopted for the remained tests with 1 GCPs, 2 GCPs, 4 GCPs and 9 GCPs. Since R-Cp model can be considered as the modification of both Konecny G model and Leberl F model, orientation experiments are also conducted on the same data using the two models for comparison. Root men square error (RMSE) values of control points and check points are calculated, as presented in Table 1, in which x is the azimuth direction and y is the range direction. Fig. 5(a) and (b) are the error vector diagrams of the check points using 1 and 13 control points with R-Cp model, respectively. The unit (pixel) of statistical precision is performed according to the sampling resolution 1.0 m instead of actual ground resolution of 2.5 m.

Table 1 Precision of image positioning with different numbers of control points/pixel

GCP Num		1	2	4	9	13
RCp GCPs	*x*	0.01	0.10	5.19	3.36	
	y	0.01	0.10	2.84	2.87	
RCp CPs	*x*	5.88	5.91	4.75	3.39	3.23
	y	5.61	4.47	3.56	2.95	2.94
Konecny GCPs	*x*	0.01	0.12	5.41	3.88	
	y	0.01	0.11	2.91	2.89	
Konecny. CPs	*x*	6.11	5.98	5.19	4.22	4.11
	y	5.75	4.55	3.60	3.20	3.06
Leberl GCPs	*x*	0.02	0.27	5.66	4.97	
	y	0.01	0.15	3.10	3.15	
Leberl CPs	*x*	7.39	6.67	6.46	5.38	5.27
	y	6.09	4.71	3.95	3.31	3.15

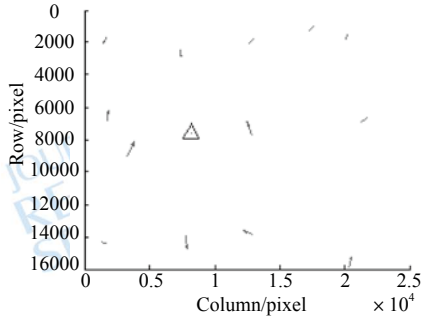

(a) One ground control point

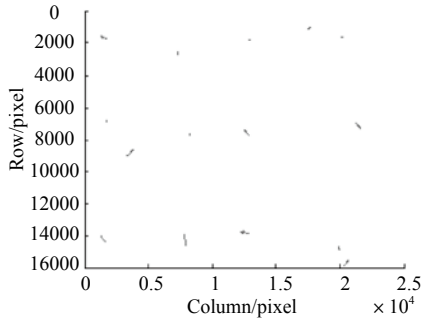

(b) Thirteen ground control points

Fig. 5 Distribution of control points and check points, and the residual error vector of various points

5.2 Stereoscopic positioning experiment

Two adjacent SAR images in different airstrips in the same experiment area as shown above are selected as stereopairs. There are 6 ground points with known coordinates in the overlapping area, as shown in Fig. 6.

During the experiment, 2 points (Point 1 and Point 5 in Fig. 6) and 5 points are selected as control points, respectively, while the remained points are used as check points, and LOOCV is adopted as precision verification method when 5 GCPs are used. Errors of all ground points in geocentric coordinate system are obtained as shown in Table 2 and Table 3.

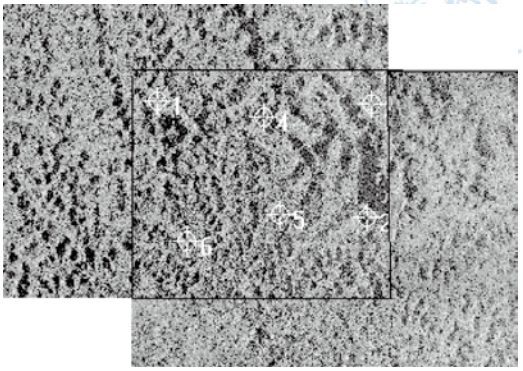

Fig. 6 Airborne SAR stereopairs

Table 2 Errors and precision with 2 GCPs /m

Attribute	Point No.	X	Y	Z
Errors of GCPs	1	– 0.19	0.28	– 0.18
	2	0.12	0.32	0.24
Errors of CPs	3	– 0.08	1.03	0.47
	4	– 2.58	0.87	2.89
	5	1.11	– 1.39	– 0.87
	6	3.57	– 1.33	– 0.06
Precision of CPs	components	2.27	1.17	1.52
	synthetical		2.97	

Table 3 Errors and precision with 5 GCPs /m

Point No.	X	Y	Z
1	– 0.09	2.44	– 1.98
2	1.71	2.22	1.11
3	0.07	1.11	0.89
4	– 1.75	0.62	2.44
5	– 0.06	– 2.09	– 0.85
6	2.33	– 1.32	0.82
Components	1.38	1.76	1.49
synthetical		2.68	

5.3 Test analysis

It can be seen from the experiment above:

(1) Similar to radar collinearity equation, R-Cp equation can achieve geometric processing of side-looking radar image by adopting exterior orientation elements as orientation parameters without knowing the imaging parameters. Without considering the precision loss of SAR image re-sampling and DEM interpolation, image orientation precision is theoretically the precision of orthorectification using DEM with the same elevation precision of check point. This indicates that when 4 control points are adopted, the precision of orthophoto is about 5.7 m, which can be calculated according to the statistical precision of azimuth/range direction of check points and

the sampling resolution of the two directions (Yuan & Wu, 2010).

(2) Comparing to all kinds of radar collinearity equations, R-Cp equation can easily achieve the forward intersection and the stereoscopic positioning of radar image. The test show that the rigorous positioning of airborne SAR image with few control points has high precision, and the difference in positioning precision is not significant when two and five control points are adopted.

(3) The orientation experiments with different models on the same SAR data indicate that the precision of R-Cp model established in this study is higher than Leberl F model and Konecny G model. This demonstrates that the R-Cp model complies with the geometric imaging mechanism of side-looking radar remote sensing image.

Due to certain differences between positioning model and geometric imaging model, the test of this study is to verify the accuracy and feasibility of the geometric imaging equation with positioning model. Meanwhile, since there are numerous imaging methods of synthetic aperture radar, any geometric equation only combined with the mechanism and process of imaging may be absolutely rigorous. From this perspective, there is no rigorous geometric imaging model which could be completely applicable to all SAR images. SAR imaging has motion compensation process. If SAR image has the same features of geometric deformation as that of the image shoot by the real aperture radar under the ideal motion state referenced by the motion compensation process, the real aperture radar-based R-Cp model established in this study can still be useful to SAR images.

6 CONCLUSION

Range equation in R-Cp equations reflects the imaging mechanism in range direction of side-looking radar image, while coplanarity equation involving the azimuth parameters of attitude reflects the imaging mechanism of azimuth direction. Compared with Leberl F model, R-Cp model proposed in this study takes into account of the influence of sensor attitude on imaging positioning of side-looking radar. The orientation parameters of R-Cp model are the same as that of radar collinearity equation model, but R-Cp model does not need to consider the conversion between range projection and central projection. As optical and radar sensors are carried on the same platform more often than ever, in this case, the same trajectory and attitude data are shared by both optical and radar sensors. Therefore, the same orientation parameters used in rigorous positioning of optical and radar remote sensing images will be beneficial for the combination processing of the two sensor images. Because the model can fully utilize high precision GPS data and IMU data of POS observation values, it could facilitate the application of POS data in high-precision geometric processing of side-looking radar images. Moreover, the concise form and easy application of this equation make it suitable to be used as the basic model in radar image photogrammetry. In order to promote more extensive applications of the model on radar image correction, stereoscopic positioning, block adjustment, mapping, matching with object-space restraint, and even on SAR imaging for different airborne or spaceborne SAR sensors, further research on the equation and related external conditions are also important.

REFERENCES

Brovelli M A, Crespi M, Fratarcangeli F, Giannone F and Realini E. 2006. Accuracy Assessment of High Resolution Satellite Imagery by Leave-one-out method. Proceedings of the 7th International Symposium on Spatial Accuracy Assessment in Natural Resources and Environmental Sciences, July, Lisbon, Portugal: 533–542

Chen E X. 2004: Study on Ortho-rectification Methodology of Spaceborne Synthetic Aperture Radar Imagery. Beijing:Chinese Academy of Forestry:11–12

Gelautz M, Frick H, Raggam J, Burgstaller J and Leberla F. 1998. SAR image simulation and analysis of alpine terrain. ISPRS Journal of Photogrammetry and Remote Sensing, 53(1): 17–38 DOI: 10.1016/S0924-2716(97)00028-2

Johnsen H, Lauknes L and Guneriussen T. 1995. Geocoding of fast-delivery ERS-1 SAR image mode product using DEM data. International Journal of Remote Sensing, 16(11): 1957–1968 DOI: 10.1080/01431169508954532

Konecny G and Schuhr W. 1988. Reliability of Radar Image Data. 16th ISPRS, (16): 92–101

Leberl F. 1978. Radargrammetry for Image Interpretation. ITC Technical Report

Leberl F. 1990. Radar image grammetric processing. Artech House

Li L G, You H J, Peng H L, Wu Y R, Liu B and Zhou Q. 2007. A new method to locate satellite SAR imagery. Journal of Electronics & Information Technology, 29(6): 1441–1444

Pang L. 2006. Study of the Triangulation Method From Airborne Synthetic Aperture Radar Images. Qingdao: Shandong University of Science and Technology: 31-41, 77–79

Shu N. 2000. Principles of Microwave Remote Sensing. Wuhan: Wuhan University Press: 116–120

Yang J, Pan B, Li D R and Zhong Y Z. 2006. Location of spaceborne SAR imagery without reference points. Geomatics and Information Science of Wuhan University, 31(2): 144–147

You H J, Ding C B and Fu K. 2007. SAR image localization using rigorous SAR collinearity equation model. Acta Geodaetica et Cartographica Sinica, 36(2): 158–162

Yuan X X and Wu Y D. 2010. Object location of space-borne SAR imagery under lacking ground control points. Geomatics and Information Science of Wuhan University, 35(1): 88–91, 96

Zhu C Y, Lan C Z, Xu Q, Wang J F and Chi T H. 2003. Geographic registration for air-bome SAR image with no ground control point supported by GPS position data. Acta Geodaetica et Cartographica Sinica, 32(3): 234–238

雷达影像几何构像距离-共面方程

程春泉[1]，张继贤[1]，邓喀中[2]，张力[1]

1. 中国测绘科学研究院，北京 100039；
2. 中国矿业大学，江苏 徐州 221116

摘 要：几何构像方程是遥感影像摄影测量最基本最重要的公式，简洁性和严密性是其能得到广泛应用的必要条件。本文分析了姿态对侧视雷达影像成像的影响，以传感器位置和姿态(外方位元素)作为定向参数，根据侧视雷达成像的距离和波束中心共面(Range-Coplanarity, R-Cp)条件构建了一种简洁严密的几何构像方程。该方程考虑了姿态参数对雷达影像严密定位的影响，反映了侧视雷达遥感影像的成像几何原理，避开了复杂的成像参数，实现了雷达影像与光学影像严密构像模型定向参数的统一。定位试验精度优于Leberl F模型和Konecny G模型。该方程的特点表明其在侧视雷达遥感影像的摄影测量领域中有着一定的应用潜力。

关键词：距离-共面方程，几何构像模型，外方位元素，侧视雷达，严密定位模型

中图分类号：P237 **文献标志码**：A

引用格式：程春泉, 张继贤, 邓喀中, 张力. 2012. 雷达影像几何构像距离–共面方程. 遥感学报，16(1): 38–49
Cheng C Q, Zhang J X, Deng K Z and Zhang L . 2012. Range-Coplanarity equation for radar geometric imaging. Journal of Remote Sensing, 16(1): 38–49

1 引 言

侧视雷达遥感影像严密构像方程主要有基于距离–多普勒方程与基于雷达共线方程模型(陈尔学，2004)。Leberl F模型(Leberl，1978，1990)依据距离条件和零多普勒条件，符合雷达成像机理，其考虑了传感器外方位元素中的线元素变化，但未考虑角元素的变化；R-D模型，原理与Leberl F方法相似，考虑了多普勒频率非零值情况，对不同像点处的多普勒频率常采用常量、线性和低阶多项式模型来描述，具有明确的几何和物理意义(Johnsen 等，1995)，以R-D模型为基础，众多学者对无控制点(朱彩英 等，2003；杨杰 等，2006)、稀少控制点(袁修孝和吴颖丹，2010)及高山地(Gelautz 等，1998; Johnsen 等，1995)SAR影像的定位进行了研究，是目前应用最广泛的模型。雷达共线方程的模型以外方位元素作为定向参数，是光学遥感影像共线方程应用的延伸。Konecny G等人提出的共线方程考虑了地形对投影点位置的影响，增加了地形对投影点位置影响的修正因子(Konecny和Schuhr，1988)；国内也有学者以雷达近似共线方程为基础，通过距离投影到中心投影的转换，对其进行修正得到雷达严密共线方程模型(尤红建 等，2007；李立钢 等，2007)，建立了基于外方位元素的雷达影像严密构像模型。

2 姿态对雷达成像影响

在R-D模型中，没有直接包含姿态参数，对滚动角是否影响侧视雷达遥感影像的严密定位，不同学者认识上有较大差距(庞蕾，2006)。本文首先对各姿态的独立影响进行简单分析，后文共面方程的推导过程中，滚动角是否影响侧视雷达影像的定位有一个清晰的结论。

图1(a)显示了3个姿态角均为0时的理想状况，以

收稿日期：2011-05-22；**修订日期**：2011-07-31

基金项目：国家自然科学基金(编号: 41071237)；国家高科技研究发展计划(863计划)(编号: 2011AA120401，2011AA120402)；国家测绘局领军人才基金(编号: A11114)

第一作者简介：程春泉(1972—)，男，博士，副研究员，主要从事遥感影像的数字摄影测量理论与应用研究工作, 已发表论文十余篇。E-mail: cspring@casm.ac.cn。

真实孔径雷达为研究对象，姿态角的变化对影像成像和定位的影响分析参考理想状态进行。

2.1 滚动角对雷达成像的影响

滚动角的存在，使得天线摄影时照准范围发生改变，但对于同一个地面点，并不改变摄影时刻天线到地面点间的距离，也不改变地面点的摄影时刻。因此，在其他姿态角不变的情况下，滚动角的改变对地面特定目标点的成像没有影响，如图1(b)。

2.2 俯仰角对雷达成像的影响

俯仰角的存在，使得特定地面目标点的摄影时刻发生变化，目标相对于摄影时刻的天线位置向前方或后方产生偏移，摄影时刻与传感器天线间的距离增大，因此，俯仰角的变化造成地面点在影像中行列方向位置都会改变，影响了影像的成像，如图1(c)。

2.3 偏航角对雷达成像的影响

偏航角的存在，使得天线的照准目标产生偏转，同一个地面点的摄影时刻发生变化，摄影时刻与传感器天线间的距离增大，因此，地面点在影像中的坐标行列方向都会改变，且行方向坐标的变化随列方向坐标不同而有明显差异，表明偏航角对雷达影像的成像有直接的影响，如图1(d)。

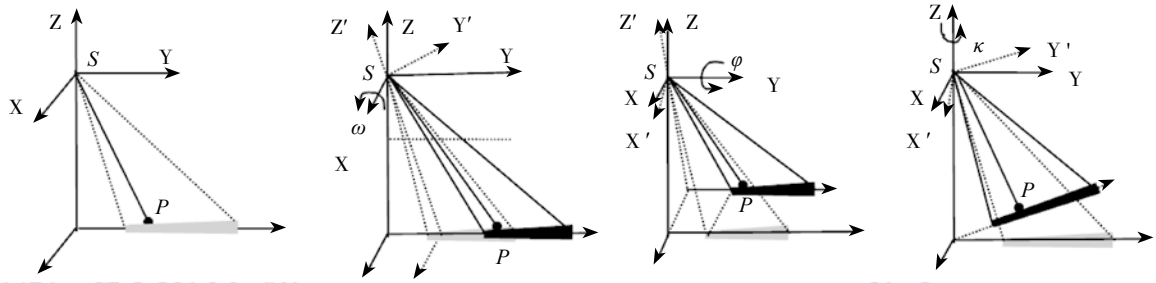

(a) 姿态角为0　(b) 滚动角影响　(c) 俯仰角影响　(d) 偏航角影响

图1　姿态角对侧视雷达影像成像影响示意图

3　侧视雷达影像定位距离–共面方程

侧视雷达有平面扫描和锥面扫描两种模式(舒宁，2000)，此处首先讨论平面扫描模式。

3.1 距离–共面(Range–Coplanarity，R–Cp)方程的基本原理

距离-共面条件是指一行影像对应的所有地面点均在该行影像摄影时刻天线发射的雷达波束扫描面内，影像行上每个像点的成像满足距离条件(图2)。本文基于传感器状态矢量和姿态参数(外方位元素)的雷达遥感影像构像方程通过传感器与地物目标间的距离条件和波束中心共面条件来构建：

(1)一行影像对应地面点及相应成像时刻的天线中心在同一个扫描波束中心面内，这个波束中心面由传感器状态矢量和姿态确定；

(2)传感器至地面目标点的空间距离与雷达波测量的距离相等。

因此，距离-共面方程可根据如下公式建立：

$$\begin{cases} R = |\overrightarrow{OP} - \overrightarrow{OS}| = \tau c / 2 \\ \vec{i} \cdot (\overrightarrow{OP} - \overrightarrow{OS}) = 0 \end{cases} \tag{1}$$

式中，$\vec{i}$、$\overrightarrow{OP}$、$\overrightarrow{OS}$分别为波束中心面的法向量(即为传感器坐标系的x轴经姿态旋转后的x'轴)、地面点位置和传感器位置向量。R为斜距，c为光速，τ为雷达波从雷达天线到目标点的往返时间。上式中第一式为距离方程，与R-D和Leberl F模型中的距离方程是相同的，第二式为雷达发射的波束中心面方程。

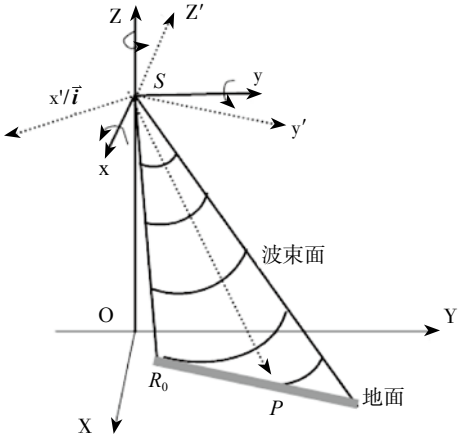

图2　侧视雷达距离共面成像几何

3.2 转角系统的选择与平面扫描模式的共面方程

姿态对侧视雷达遥感影像定位的影响前文进行了分析，但是对3个姿态角独立进行研究的。研究的结论为φ、κ角影响地面点的成像，ω角只影响侧视雷达的测绘范围，不影响地面点在影像上的位置。由于欧拉角的后次转角是在前次转角的基础上进行，ω角是否影响雷达影像的定位，与转角顺序还存在关系。欧拉角的转角顺序有6种，在光学影像定位领域，ω-φ-κ是国际上比较通用的转角系统，但这种转角顺序在建立雷达影像的波束扫描面方程时却不是最佳的，以下的公式推导中可以得到说明。

3.2.1 ω-φ-κ系统确定的扫描平面

以X-Y-Z轴作为转角次序的ω-φ-κ系统，本体坐标系到物方参考坐标系转换的旋转矩阵为：

$$\boldsymbol{R}_b^A = \boldsymbol{R}_X(\omega)\boldsymbol{R}_Y(\varphi)\boldsymbol{R}_Z(\kappa) \tag{2}$$

由于扫描平面的法线与姿态旋转后的传感器坐标系x'轴一致，可得其在物方坐标系中的单位向量为：

$$\vec{\boldsymbol{i}} = \boldsymbol{R}_b^A\begin{bmatrix}1\\0\\0\end{bmatrix} = \begin{bmatrix}\cos\varphi\cos\kappa\\ \cos\omega\sin\kappa+\sin\omega\sin\varphi\cos\kappa\\ \sin\omega\sin\kappa-\cos\omega\sin\varphi\cos\kappa\end{bmatrix} \tag{3}$$

将式(3)代入式(1)，并分别用(X_S，Y_S，Z_S)及(X，Y，Z)表示传感器及地面点的空间坐标，则有：

$$(X-X_S)\cos\varphi\cos\kappa+(Y-Y_S)(\cos\omega\sin\kappa+\sin\omega\sin\varphi\cos\kappa)+(Z-Z_S)(\sin\omega\sin\kappa-\cos\omega\sin\varphi\cos\kappa)=0 \tag{4}$$

3.2.2 φ-κ-ω系统确定的扫描平面

依次以Y-Z-X轴作为转角次序的φ-κ-ω转角系统，其姿态旋转矩阵为：

$$\boldsymbol{R}_b^A = \boldsymbol{R}_Y(\varphi)\boldsymbol{R}_Z(\kappa)\boldsymbol{R}_X(\omega) \tag{5}$$

物方坐标系中波束扫描面法线单位向量为：

$$\vec{\boldsymbol{i}} = \boldsymbol{R}_b^A\begin{bmatrix}1\\0\\0\end{bmatrix} = \begin{bmatrix}\cos\varphi\cos\kappa\\ \sin\kappa\\ -\sin\varphi\cos\kappa\end{bmatrix} \tag{6}$$

将式(6)代入式(1)中的共面方程，有展开式：

$$(X-X_S)(\cos\varphi\cos\kappa)+(Y-Y_S)\sin\kappa-(Z-Z_S)(\sin\varphi\cos\kappa)=0 \tag{7}$$

同样可证明当采用κ-φ-ω转角系统时，与式(7)一样，共面方程也不含ω参数。

3.2.3 平面扫描模式的侧视雷达距离–共面方程

距离-共面方程中的距离方程与距离-多普勒方程的距离方程完全一样，与式(7)一起，形成基于φ-κ-ω转角系统的斜距距离-共面方程：

$$\begin{cases}(X-X_S)(\cos\varphi\cos\kappa)+(Y-Y_S)\sin\kappa-(Z-Z_S)(\sin\varphi\cos\kappa)=0\\ (X-X_S)^2+(Y-Y_S)^2+(Z-Z_S)^2=(y_sM_y+R_0)^2\end{cases} \tag{8}$$

式中，M_y为距离向采样分辨率，R_0为初始斜距，y_s为像元在影像上的列坐标。

从共面方程的推导可以看出，当使用ω-φ-κ转角系统时，ω角对影像定位是有影响的，当采用φ-κ-ω转角系统时，ω角对影像定位没有影响。采用φ-κ-ω转角系统的距离-共面方程是以3个线元素和两个角元素作为定向参数构建的。姿态为不同的值时，共面条件表达了经过摄影时刻传感器天线中心不同面的集合，当面垂直于传感器速度方向时，即为Leberl F模型。因此，可以认为Leberl F模型是距离-共面方程模型的一个特例。

相同的传感器状态矢量(位置和速度)和地形条件下，不同的传感器姿态会产生不同的多普勒频率，姿态参数和多普勒参数间是可以转换的。与所有类型的雷达共线方程一样，R-Cp模型以姿态作为参数，影像几何处理与多普勒频率、雷达波长等参数并不存在直接的关系，表明其避开成像参数即可进行侧视雷达遥感影像的几何处理。对于非正侧视雷达影像，一行影像不同列坐标的像点有不同的多普勒频率值，但却仅有一组相同的姿态角，表明R-Cp模型与R-D模型间既存在联系，又存在区别。

3.3 圆锥扫描雷达构像方程

当侧视雷达按圆锥扫描方式工作时，雷达波束有一个固定的航向倾角τ，并且绕天线轴作圆锥扫描，如图3 (舒宁，2000)。对于任意一地面点**P**，其必然在扫描锥面上，且该点到传感器**S**的距离等于**R**。锥面方程表达该面上的所有地面点与天线位置构成的向量$\vec{\boldsymbol{r}}$与旋转轴向量$\vec{\boldsymbol{i}}$构成的夹角为90° – τ，其数学表达式为：

$$\cos(\vec{\boldsymbol{i}},\vec{\boldsymbol{r}}) = \cos(\pi/2-\tau) = \sin(\tau) = \frac{\vec{\boldsymbol{i}}\cdot\vec{\boldsymbol{r}}}{|\vec{\boldsymbol{i}}||\vec{\boldsymbol{r}}|} \tag{9}$$

采用φ-κ-ω转角系统时，式(9)中转轴单位向量$\vec{\boldsymbol{r}}$用式(6)代入，即获得相应圆锥扫描雷达影像的构像方程展开式：

$$\begin{cases}\cos\varphi\cos\kappa(X-X_S)+\sin\kappa(Y-Y_S)-\\ \sin\varphi\cos\kappa(Z-Z_S)-(y_sM_y+R_0)\sin\tau=0\\ (X-X_S)^2+(Y-Y_S)^2+(Z-Z_S)^2-(y_sM_y+R_0)^2=0\end{cases} \tag{10}$$

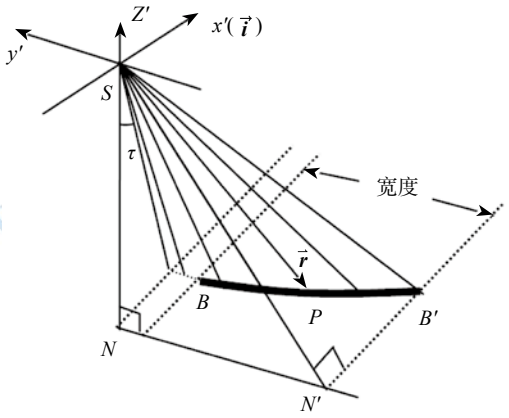

图3 圆锥扫描雷达影像的成像几何

由于这种扫描方式相对来说较少见，作者在此处仅给出基本方程，不作深入讨论，以下默认为平面扫描模式成像。

4 侧视雷达遥感影像严密定位模型

试验以式(8)即为基础，以外方位元素和地面点坐标增量作为未知参数并线性化，形成误差方程的一般形式：

$$\begin{cases} v_1 = f_{1X_S}\delta_{X_S} + f_{1Y_S}\delta_{Y_S} + f_{1Z_S}\delta_{Z_S} + f_{1\varphi}\delta_\varphi + \\ \quad f_{1\kappa}\delta_\kappa + f_{1X}\delta_X + f_{1Y}\delta_Y + f_{1Z}\delta_Z - l_1 \\ v_2 = f_{2X_S}\delta_{X_S} + f_{2Y_S}\delta_{Y_S} + f_{2Z_S}\delta_{Z_S} + f_{2\varphi}\delta_\varphi + \\ \quad f_{2\kappa}\delta_\kappa + f_{2X}\delta_X + f_{2Y}\delta_Y + f_{2Z}\delta_Z - l_2 \end{cases} \tag{11}$$

式中，v_1、v_2分别代表式(8)中的距离和共面模型对应的误差方程；$f_{..}$代表距离共面方程线性化的系数，δ代表增量未知数，其下标X_s、Y_s、Z_s、φ和κ代表外方位元素，X、Y和Z代表地面点坐标；l_1、l_2代表误差方程式常量。

外方位元素的精化模型一般采用低阶多项式，即：

$$P_i = P_{i0} + a_{i0} + a_{i1}t + a_{i2}t^2 + \cdots + a_{in}t^n (i=1, 2, 3, 4, 5) \tag{12}$$

P_i、P_{i0} (i=1, 2, 3, 4, 5)分别代表位置和姿态(X、Y、Z、φ和κ)的精化值和初值，(a_{i0}，a_{i1}，a_{i2}，…，a_{in})代表一般多项式系数。

将距离共面方程、地面点坐标、轨道和姿态精化模型相关的误差方程式一起，形成以下方程组：

$$\begin{cases} \boldsymbol{V}_{12} = \boldsymbol{B}_g\boldsymbol{g} + \boldsymbol{B}_t\boldsymbol{t} - \boldsymbol{L}_{12} & \boldsymbol{P}_{12} \\ \boldsymbol{V}_g = \boldsymbol{E}_g\boldsymbol{g} - \boldsymbol{L}_g & \boldsymbol{P}_g \\ \boldsymbol{V}_t = \boldsymbol{E}_t\boldsymbol{t} - \boldsymbol{L}_t & \boldsymbol{P}_t \end{cases} \tag{13}$$

式中，$\boldsymbol{V}_{12}$、$\boldsymbol{V}_g$和$\boldsymbol{V}_t$分别为距离共面条件、地面点坐标、POS精化模型相关的观测值或虚拟观测值改正向量；$\boldsymbol{g}$代表地面点坐标增量未知数向量[ΔX，ΔY，ΔZ]，$\boldsymbol{t}$代表轨道(航迹)姿态精化模型的一般多项式系数未知数向量[a_{i0}，a_{i1}，a_{i2}，…，a_{in}]；$\boldsymbol{L}_{12}$、$\boldsymbol{L}_g$、$\boldsymbol{L}_t$为相应观测值误差方程常数向量；$\boldsymbol{B}_g$、$\boldsymbol{B}_t$、$\boldsymbol{E}_g$、$\boldsymbol{E}_t$为误差方程系数设计矩阵；$\boldsymbol{P}_{12}$、$\boldsymbol{P}_g$、$\boldsymbol{P}_t$为权矩阵。

5 试 验

构像方程的应用几乎涉及遥感影像摄影测量的各个领域，本文仅通过定位模型对该构像方程的正确性和可行性进行检验，定向和定位使用的联合平差误差方程组为式(13)，即基于φ-κ-ω转角系统的R-Cp构像方程构建，定向参数通过最小二乘解算，检查点坐标理论值根据计算得到的定向参数计算，检查点精度根据理论值和实测值间的误差统计获得。本文采用的机载SAR试验数据获取于2006年6月成都地区，像元方位向和距离向采样分辨率大小为1.0 m，实际地面分辨力约为2.5 m。POS系统为加拿大Applanix公司的AV510，由于集成初期POS与传感器间的时间同步误差较大，作者将POS测量值加上常数(即平移)进行粗差修正后作为观测初值，而姿态初始值设为0。

5.1 单景影像定向试验

影像区域内共有14个坐标已知的地面点，通过高分辨率光学航空影像空3加密获取，其原始影像与地面点的分布如图4所示。

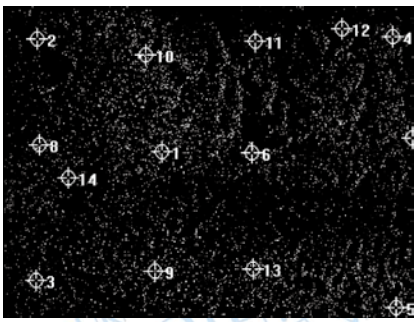

图4 原始机载SAR影像

影像定向试验控制点分别采用1个(中间1号点位置)、2个(左上、右下角控制)、4个(4角控制)、9个(3行3列控制)和13个控制点(舍一交叉法精度验证(Brovelli 等，2006)，将所有地面点依次作为检查点)。13个控制点时，航迹姿态采用二次多项式精化模型，其余均采用线性精化模型。由于R-Cp模型可

以看作是Konecny G模型及Leberl F模型的改进，为了对比，相同的数据也采用Konecny G模型和Leberl F模型进行定位试验，解算后得到各控制点和检查点的中误差，统计于表1中，其中x代表方位向，y代表距离向。统计精度的单位像元按原始影像1.0 m采样分辨率而非实际地面分辨率2.5 m归算。图5(a)，(b)分别显示了利用本文模型在1个和13个控制点定向时检查点的误差矢量图。

表1 不同数目控制点影像定向精度/像元

控制点数		1	2	4	9	13
R Cp 控制点	x	0.01	0.10	5.19	3.36	
	y	0.01	0.10	2.84	2.87	
R Cp 检查点	x	5.88	5.91	4.75	3.39	3.23
	y	5.61	4.47	3.56	2.95	2.94
Konecny G 控制点	x	0.01	0.12	5.41	3.88	
	y	0.01	0.11	2.91	2.89	
Konecny G 检查点	x	6.11	5.98	5.19	4.22	4.11
	y	5.75	4.55	3.60	3.20	3.06
Leberl F 控制点	x	0.02	0.27	5.66	4.97	
	y	0.01	0.15	3.10	3.15	
Leberl F 检查点	x	7.39	6.67	6.46	5.38	5.27
	y	6.09	4.71	3.95	3.31	3.15

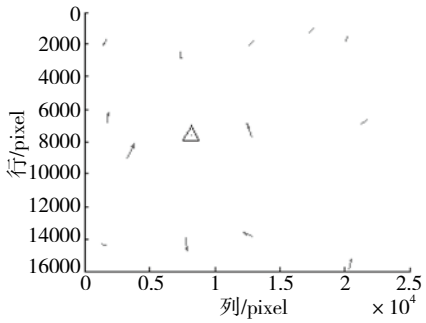

(a) 1个控制点

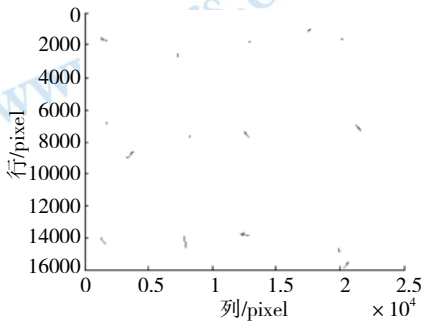

(b) 13个控制点

图5 控制点和检查点分布及各点定向残差矢量

5.2 立体定位试验

选取同一测区不同航带的两张相邻SAR影像作为立体像对，重叠区内共有6个已知地面点，如(图6)所示：

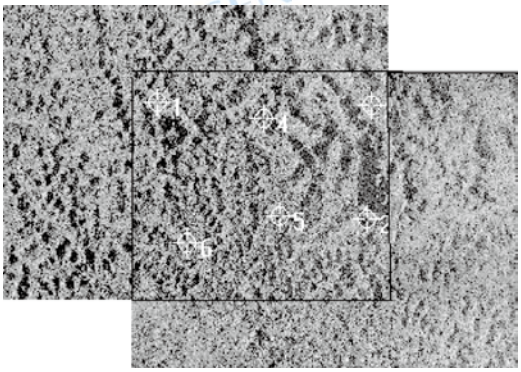

图6 机载SAR立体像对

试验时，分别采用2个(图6中1和2点)和5个点作为控制点，其余作为检查点，其中5个控制点时采用舍一精度验证法进行精度验证(Brovelli 等，2006)，得到各点在地心直角坐标系中的误差统计于表2、表3部分。

表2 2GCPs各地面点误差和统计精度 /m

点属性	点号	X	Y	Z
控制点误差	1	– 0.19	0.28	–0.18
	2	0.12	0.32	0.24
检查点误差	3	– 0.08	1.03	0.47
	4	– 2.58	0.87	2.89
	5	1.11	– 1.39	– 0.87
	6	3.57	– 1.33	– 0.06
检查点精度	分量	2.27	1.17	1.52
	合成		2.97	

表3 5GCPs各地面点误差和统计精度(舍一法精度验证)/m

点号	X	Y	Z
1	– 0.09	2.44	– 1.98
2	1.71	2.22	1.11
3	0.07	1.11	0.89
4	– 1.75	0.62	2.44
5	– 0.06	– 2.09	– 0.85
6	2.33	– 1.32	0.82
分量	1.38	1.76	1.49
合成		2.68	

5.3 试验分析

从上面的试验可以看出：

(1)距离共面方程可以与雷达共线方程一样，以外方位元素作为定向参数无需知道成像参数即可实现单景侧视雷达影像的几何处理，在不考虑重采样精度和DEM内插精度损失的情况下，理论上单景影像定向精度与利用检查点高程相同精度的DEM进行正射纠正的精度一致，即当采用4个控制点时，根据检查点方位向和距离向统计精度以及两方向的采样分辨率，归算为影像正射纠正精度(袁修孝和吴颖丹，2010)约为5.7 m；

(2)与各种形式的雷达影像共线方程相比，距离共面方程更容易实现雷达影像的前方交会和雷达影像的立体定位，试验表明，稀少控制点的机载SAR影像立体定位有较好的精度，采用2个和5个控制点时，定位精度差别不显著；

(3)相同SAR影像的定向试验表明，本文所建立的距离共面模型精度要优于Leberl F模型和Konecny G模型，表明R-Cp模型更符合侧视雷达遥感影像的成像机理，有更好的严密性。

由于定位模型与构像模型间还存在很大的差异，本文试验的目的是利用定位模型来论证构像方程的正确可行性。同时，由于合成孔径雷达的成像方式众多，任何定位模型均需跟成像机理、过程结合起来才有可能真正的严密，从这个意义上说目前还没有一个完全适用于所有SAR影像严密几何构像模型。SAR在成像中有运动补偿过程，如果SAR影像仍具有真实孔径雷达在补偿时参考的理想运动状态下获得的影像相同的几何形变特点，本文基于真实孔径雷达建立的R-Cp模型仍然可以用于SAR影像。

6 结 论

R-Cp方程中的距离方程反映了侧视雷达影像距离向的成像机理，包含了姿态方位角参数的共面方程则反映了方位向的成像机理。与Leberl F模型相比，考虑了姿态对侧视雷达影像定位的影响；与各种形式的雷达共线方程相比，定向参数相同，但不用考虑距离投影与中心投影的转换，无需额外增加地形影响因子的修正。由于同一平台同时搭载光学与雷达传感器日益普遍，同平台传感器影像具有相同的轨道(轨迹)、姿态数据，光学与雷达遥感影像的严密定位使用相同的定向参数，无疑会有利于光学与侧视雷达遥感影像的联合处理。同时，该模型能充分利用当代高精度POS观测值中的GPS数据与IMU数据，有利于促进POS数据在侧视雷达影像高精度几何处理中的应用。加上该方程形式简洁，使用方便，适合作为摄影测量的基础模型。因此，值得对该方程及其关联的外部条件进一步研究，使其在不同机、星载侧视雷达传感器遥感影像的纠正、立体定位、区域网平差、测图、物方约束的匹配以及SAR成像领域中发挥作用。

参考文献(References)

Brovelli M A, Crespi M, Fratarcangeli F, Giannone F and Realini E. 2006. Accuracy Assessment of High Resolution Satellite Imagery by Leave-one-out method. Proceedings of the 7th International Symposium on Spatial Accuracy Assessment in Natural Resources and Environmental Sciences, July, Lisbon, Portugal: 533–542

陈尔学. 2004. 星载合成孔径雷达影像正射纠正方法研究. 北京：中国林业科学研究院: 11–12

Gelautz M, Frick H, Raggam J, Burgstaller J and Leberla F. 1998. SAR image simulation and analysis of alpine terrain. ISPRS Journal of Photogrammetry and Remote Sensing, 53(1): 17–38 DOI: 10.1016/S0924–2716(97)00028–2

Johnsen H, Lauknes L and Guneriussen T. 1995. Geocoding of fast-delivery ERS-1 SAR image mode product using DEM data. International Journal of Remote Sensing, 16(11): 1957–1968 DOI: 10.1080/01431169508954532

Konecny G and Schuhr W. 1988. Reliability of Radar Image Data. 16th ISPRS, (16): 92–101

Leberl F. 1978. Radargrammetry for Image Interpretation. ITC Technical Report

Leberl F. 1990. Radar image grammetric processing. Artech House

李立钢, 尤红建, 彭海良, 吴一戎, 刘波, 周强. 2007. 一种新的星载SAR图像定位方法的研究. 电子与信息学报, 29(6): 1441–1444

庞蕾. 2006. 机载合成孔径雷达空中三角测量方法的研究. 青岛: 山东科技大学: 31–41,77–79

舒宁. 2000. 微波遥感原理. 武汉: 武汉大学出版社: 116–120

杨杰, 潘斌, 李德仁, 钟永正. 2006. 无地面控制点的星载SAR影像直接对地定位研究. 武汉大学学报(信息科学版), 31(2): 144–147

尤红建, 丁赤飚, 付琨. 2007. SAR图像对地定位的严密共线方程模型. 测绘学报, 36(2): 158–162

袁修孝, 吴颖丹. 缺少控制点的星载SAR遥感影像对地目标定位. 武汉大学学报(信息科学版), 2010, 35(1): 88–91, 96

朱彩英, 蓝朝桢, 徐青, 王劲峰, 池天河. 2003. GPS支持下的机载SAR遥感图像无控制准实时地理定位. 测绘学报, 32(3): 234–238